Tribol Lett (2010) 37:313–326
DOI 10.1007/s11249-009-9525-4

ORIGINAL PAPER

Microtribology and Friction-Induced Material Transfer in Layered MoS_2 Nanoparticles Sprayed on a Steel Surface

Rashmi R. Sahoo · Sanjay K. Biswas

Received: 24 April 2009 / Accepted: 21 September 2009 / Published online: 2 October 2009

Abstract Frictional performance of molybdenum disulfide (MoS_2) particles sprayed on a substrate is investigated in a ball-on-disc tribometer. The ability of large ($\sim$2 μm) and small ($\sim$50 nm) particles to generate low-friction transfer film is investigated with a view to elucidate the requirement for film formation. Particle migration, particle stability in the contact region, oxidation potential, and particle adhesion to the substrate are explored within a span of operating parameters; normal load, and sliding velocity. It is found that the larger particles are able to migrate to the contact to raise a homogeneous but nonuniform low-friction transfer film that flows plastically to yield large contact areas, which aid in wear protection. Within the present load and speed range, the inability of small particles to stay in the contact region and undergo basal slip militates against the formation of a low-friction transfer film.

Keywords MoS_2 · Nanotribology · Raman spectroscopy · Transfer film · Friction · Solid lubricant

1 Introduction

Layered materials such as graphite, MoS_2, and WS_2 (platelets of the 2H polytype) are used both as solid lubricants [1, 2] and as additives in liquid lubricants [3, 4]. A liquid such as oil or water perform well as a lubricant in the hydrodynamic regime where the viscosity of the liquid controls friction. The load bearing capacity of most liquids is limited and their performance is impaired in the boundary regime where direct contact occurs between mating parts promoting high friction and wear. Organic boundary lubricant additives may be used to functionalize the mating parts to prevent direct contact. The other option is to use solid lubricant such as graphite or metal dichalcogenides, which have high thermal stability and good load bearing property [5–16]. These materials generally have a layered structure, which shear easily under traction to yield low frictional forces. The low friction of both graphite and metal dichalcogenides is usually due to interplanar mechanical weakness, intrinsic to their crystal structures [17–20]. Metal dichalcogenides of the form MX_2 (M = W, Mo; X = S, Se) have a characteristic anisotropic layered structure, with M–X atoms covalently bonded in planar hexagonal arrays with each M atom surrounded by a trigonal prism of X atoms. Strong covalent forces bind M and X atoms within a lamella, whereas adjacent lamellae interact through relatively weak van der Waals forces. The unit cell has hexagonal symmetry and includes two adjacent lamellae (2H arrangement). This graphite like structure is considered to be responsible for the lubricative properties of these materials, because the weak interlamellar bonding facilitates the shear when the direction of sliding is parallel to the planes of the material.

Under the action of a shear force, intracrystalline slip occurs in the weak interplanar regions. This mechanism is responsible for the formation of smooth transfer films by wear. The new surfaces, created by separating the weakly bonded sandwiches can easily slide back and forth over one another (by intercrystalline slip), thereby providing lubrication. Coatings of Mo and W dichalcogenides were reported to be effective solid lubricants [21], which exhibit a prolonged wear life. The tribological properties were shown to be highly sensitive to the atmosphere due to chemical reactions with oxygen and water under shearing conditions

R. R. Sahoo · S. K. Biswas (✉)
Department of Mechanical Engineering, Indian Institute of Science, Bangalore 560012, India
e-mail: skbis@mecheng.iisc.ernet.in

[22, 23]. While the low friction of metal chalcogenide solid lubricants is often explained by the facile shear of the *c*-planes of the 2H lattice, this mechanism cannot explain their unusually long wear life, which has been attributed to transfer of the solid lubricant to the opposite surface via 'third body' generator processes (processes that involve materials generated within the sliding contact [24–27]).

Unfortunately, pure 2H–MoS_2 powders, however, has a short lifetime and considerably higher friction when it is used in humid, oxygen containing environments. The 2H platelets tend to stick to the mating metal components through the reactive dangling bonds on the prismatic edges. This leads to their rapid annihilation through burnishing and oxidation. It has been reported that both friction and wear increase with decreasing size of the 2H platelets [28, 29]. This observation is in agreement with the suggestion that dangling bonds mediate friction in metal dichalcogenides: as the average size of the platelets decreases, the total surface area and hence the amount of dangling bonds on the reactive surface increases. In the past few years, inorganic fullerene-like (IF) supramolecules of metal dichalcogenide MX_2 (M = Mo, W; X = S), materials with structures closely related to nested carbon fullerenes and nanotubes have been synthesized [30, 31]. Recent experiments showed that IF possesses lubricating properties superior to those of 2H platelets in a wide range of operating conditions due to its chemical inertness and to the hollow cage structure, this leads to high elasticity and may allow the particles to roll rather than slide in appropriate loading regimes. However, the effect of the inorganic fullerene-like materials as boundary lubricant decreases at high loads and sliding velocities and this has been attributed to the presence of voids and defects in the IF and the aggregation of the nanoparticles in the ambient humidity [29]. Also it has been reported that for low load, the IF material outperformed the 2H platelets, whereas at high load, the performance of the 2H lubricant is better than that of the IF [29, 32]. However, at high pressure applications [33], outer layers of these IF particles exfoliate and from in situ Raman spectra measurements it is shown that at a Hertzian pressure of 1 GPa, the IF particles transform to 2H particles.

The purpose of the present work is to come to an understanding as to what are the principal materials and process requirements that optimize the performance of these solid lubricant particles. One of the main issues involved in the use of nanoparticles in liquid suspension, as a lubricant is the ability of these particles to migrate into the region of contact. If these particles roll or shear easily when captured in contact the expected frictional forces are low. The size of the particles, their adhesion to the mating solid surface, the viscosity of the fluid, the normal load, and sliding velocity are factors, which may be expected to play roles in the transport of these particles to the region of contact. Once in this region a particle has to stay there to allow shear. This requires the particle to be anchored to the solid surface by force of adhesion. Once sheared there may be a process of transfer film formation on both the surfaces. If that happens subsequent low stress sliding may take place between the two halves of the particle or between films transferred to the substrate and the counterface. The interaction may also release debris, which goes on to the sliding track on pressing, especially if they are able to adhere to the solid substrate, a low shear coating may form on the substrate: while very big particles may have problems getting into the narrow confines of the contact, if the original particles or the debris are too small they may be swept away from the region of contact or they may get easily oxidized and loose their antifriction property. Thus, particle size, thermal stability, adhesion properties, and load become important parameters, which should dictate the performance of these layered solid lubricant particles.

When the particles are suspended in liquid, on sliding some migrate to the substrate. The particles now situated on the substrate provide a reservoir of soft matter on the surface. This matter intervenes between the mating asperities and the substrate to transmit power and dissipate energy. In this article, we investigate the process by spraying a reservoir of soft matter on the substrate and explore the process of the resulting tribology. MoS_2 particles are sprayed on a steel substrate and we track their transport, availability for shear at contact and formation of transfer film/coating, by sliding a steel ball on the sprayed particles, under dry conditions. We seek thereby explanation for the effects of particle size and normal load on tribology of these particles.

2 Experimental Details

2.1 Materials

Polycrystalline EN-31 steel (carbon 1%, manganese 1.1%, silicon 0.1%, phosphorus 0.05%, sulfur 0.05%, chromium 1%, rest iron) is used as substrates in our experiments. The layered MoS_2 particles were procured from Alfa Aesar MA, USA (2 μm avg. particle size, bigger particle) and lower friction lubricants, M. K. Impex, Canada (50 nm avg. particle size, smaller particle). Hexadecane (>99%, Sigma-Aldrich) is used as the base oil for lubricated tribology (particles suspended in hexadecane).

2.2 Preparation of Samples for AFM and Microtribometry Tests

A suspension of 20 mg of MoS_2 particles is prepared in 10 mL *n*-hexane (99.8% pure, s.d. fine chemicals limited,

Mumbai) solution and sonicated for 15 min. For the LFM experiments, a drop (2% w/v) of polymethyl methacrylate (PMMA, Mol. Wt. ~495,000) dissolved in chloroform ($CHCl_3$, 99% pure, S.D. fine chemicals limited, Mumbai) is poured on the on the 10 mm × 10 mm × 0.5 mm square p-type silicon wafer (100) substrate (R.M.S. of surface roughness = 0.2–0.3 nm) and spin coated at a rotational speed of 400 rpm. Then, the particle suspension was poured on the PMMA layer and spin coated. Then, the sample is heated to 150 °C in an oven so that the PMMA layer melt and act as an adhering layer for the MoS_2 particles. This is done carefully to ensure that, except for a small region at the bottom, the particle remains uncovered by the PMMA.

The EN-31 steel was machined and ground to give sample dimensions, 30 × 10 × 5 mm^3. The samples were then polished using 220, 320, 400, 600, 800, 1,000, 1,200 and 1,500 grit silicon carbide papers. After polishing, the samples were rinsed in acetone (AR Grade, s d fine-chem, India) and then disc was polished using diamond paste of grade 1–3 μm followed by 0.5 μm. The polished samples were cleaned by ultrasonication in acetone to remove all polishing debris. The MoS_2 were spin coated onto the steel substrate from a suspension in *n*-hexane and were stored in a desiccator prior to subjecting them to dry tribological characterization. For the lubricated tribology, microtribometric experiments were done by placing a 25 μl of MoS_2 particle suspension in hexadecane (>99%, Sigma-Aldrich) on the steel substrate. After the dry tribological tests, the samples were stored in a desiccator for further spectroscopic and microscopic characterization of the tracks created in the nanotribometer.

2.3 Tribological Tests

Two types of tribological tests were carried out: (1) lateral force microscopy (LFM) (Explorer AFM, Thermo Microscope, Santa Barbara, USA)—Si_3N_4 tips of 20-nm tip radius mounted on a cantilever of stiffness 0.15 N/m were used to generate a mean Hertzian pressure range of 1.35–5.3 GPa; (2) nanotribometer (CSM Instruments, Switzerland)—2-mm diameter 100Cr6 steel ball mounted at the end of a normally loaded cantilever was used to generate a mean Hertzian pressure range of 200–1200 MPa.

2.4 Atomic Force Microscopy

Adhesion and LFM experiments were performed using an Explorer AFM (Thermo Microscopes, Santa Barbara, U.S.A.) with Si_3N_4 cantilevers (Veeco, USA) that have pyramidal tips of a nominal end radius of 20 nm, under ambient condition (21 °C, relative humidity 35–45%). A V-shaped cantilever (normal force constant, 0.15 Nm^{-1}) was used to measure normal and lateral forces. All the tips were cleaned in a UV chamber (Bioforce Nanosciences, USA) for 20 min before use. For friction force measurement, as already reported earlier [31], we considered the difference in lateral force images recorded in the forward and reverse scans, and we report here an average of this difference. The lateral force was recorded using 1 μm × 1 μm scan area.

2.5 AFM Cantilever Calibration

We used a straightforward finite element (FEM) based technique [34] to estimate the torsional or lateral stiffness of the 'V'-shaped cantilever that is used here. This method does not require a 'multiple cantilever' (where one cantilever is of rectangular geometry) (Green et al. [35]), additional mass (Cleveland et al. [36]) or a well-defined scanning geometry (wedge calibration method [37]). The normal sensor (NR) response (A/m) is recorded from the repulsive part of the force distance curve. Known the normal cantilever stiffness (N/m) from the manufacturer and the current geometry during an experiment we estimate the normal force.

Writing an angular response AR = NR × *L*, where *L* is the length of the cantilever, the twist angle ϕ is recorded as LRA/AR, where LRA is the twist current. Known the real geometry of the cantilever (from scanning electron microscopy (SEM) images) and the material properties of the cantilever, the FEM (ABAQUS) is used to determine the torsional stiffness T/ϕ. The torque T is estimated for known ϕ. For the present cantilever, the manufacturer specifies the normal stiffness = 0.15 N/m. The FEM estimation gives $T/\phi = 1.6 \times 10^{-9}$ Nm/rad. The ratio of (T/ϕ)/Normal stiffness = 10^{-8} m^2/rad compares with those reported by Green et al. who used the Sader method (2.2×10^{-8} m^2/rad) and that formulated by Cleveland et al. (2.3×10^{-8} m^2/rad) to calibrate 'V'-shaped cantilevers.

2.6 Microtribometry (MTR)

Tribological experiments were carried out in the range 20–700 mN using a nanotribometer (CSM Instruments, Switzerland). The nanotribometer is composed of three stepper motors (two in *X*- and *Y*-axis linked to pin-on-disc module and one in *Z*-axis linked to measuring head). The cantilever was mounted on the measuring head. A 2-mm diameter steel ball (rms (root mean square) roughness ~ 1–2 nm) is attached to the end of the cantilever. Before attachment, the steel ball was cleaned in acetone using an ultrasonic bath. Two optical sensing mirrors placed near to the cantilever head, perpendicular to each other (*X*- and *Z*-axis), to measure the displacement of the cantilever during sliding against the substrate. The friction coefficient was determined during sliding by noting the deflection of the cantilever in both horizontal and vertical planes. All measurements were carried out in reciprocating mode

under ambient conditions (relative humidity: 35–45%, temperature: 295 K).

2.7 NTR Track Analysis

To explore the status of the particle in the slid track of the NTR, the samples were subjected to further investigation. Microscopic features of the samples were obtained using scanning electron microscopy (SEM, FEI, Sirion). Section distributions of the elements was performed with energy dispersive spectroscopy (EDS). Surface roughness was characterized using WYKO NT1100 optical profiling system. The effective field of view was 610 μm × 464 μm at 10× effective magnifications. The roughness parameters were measured using Veeco (vision32) software.

Resonance Raman spectra were recorded at room temperature using a standard backscattering geometry applied with Renishaw inVia reflex micro Raman spectrometer. Excitation wavelength of 785 nm was produced by a near IR diode laser source capable of supplying 300 mW of power. Several locations of each sample were probed to ensure reproducibility of the data. In order to prevent damage to the samples, different optical filters were used to reduce the incident power. The spectrometer was calibrated by Si line at 520 cm^{-1}.

3 Results

3.1 Sliding Experiments

3.1.1 Friction

The well-known friction modification properties of MoS_2 are utilized in practical applications by suspending the particles in oils and greases [5–16]. What is of interest to a lubrication designer is the selection of particle size. A reduction in size on the one hand may facilitate a better distribution and transport of the particle in the medium. On the other hand, a size reduction may give rise to agglomeration [38, 39] and easy oxidation [40], phenomena, which are known to be detrimental to tribology [38, 39] as they enhance both friction and wear. Figure 1 reports microtribometric experiments done in a ball-on-flat configuration, the contact lubricated by MoS_2 suspended in hexadecane oil. It is clearly seen that over a wide range of speed and load, the friction coefficient recorded with a liquid lubricant carrying large 2 μm size particles is significantly lower than that carrying small 50 nm particles. Higher loads and higher velocities are also seen to consistently yield lower frictional coefficient. This article is devoted to explore the rationale of these effects.

To aid this investigation, we simplify the problem first by conducting dry tribological experiments on particles sprayed on a steel substrate. Figure 1 clearly shows that the trends observed in lubricated sliding are identically reproduced in the dry experiments. That being so, it provides an opportunity to seek mechanistic explanations for particle level deformation in tribology by conducting the experiments without any liquid lubricants. To follow this exploration, we go one more step further and conduct scratch experiments on single 20 μm particles and a 20-μm agglomerate consisting of small 50 nm particles.

Figure 2 shows the SEM images of large (2 μm average size) and small (50 nm average size) particles. The large particles are seen to be well differentiated from each other. Figure 2b shows lamellar structure of the large particle, each lamella has a 50–60 nm thickness. Figure 2c shows the agglomerated state of the small particles. The agglomerate diameters are found to vary between 1 and 20 μm.

The friction properties of individual particles on a substrate were measured in the LFM configuration (contact pressure in GPa regime). The LFM performed using a silicon nitride (Fig. 3a) and Si tip (Fig. 3b) showed the friction of a large particle (the tip moves parallel to the basal plane) to be always less than that of the small particle. The LFM

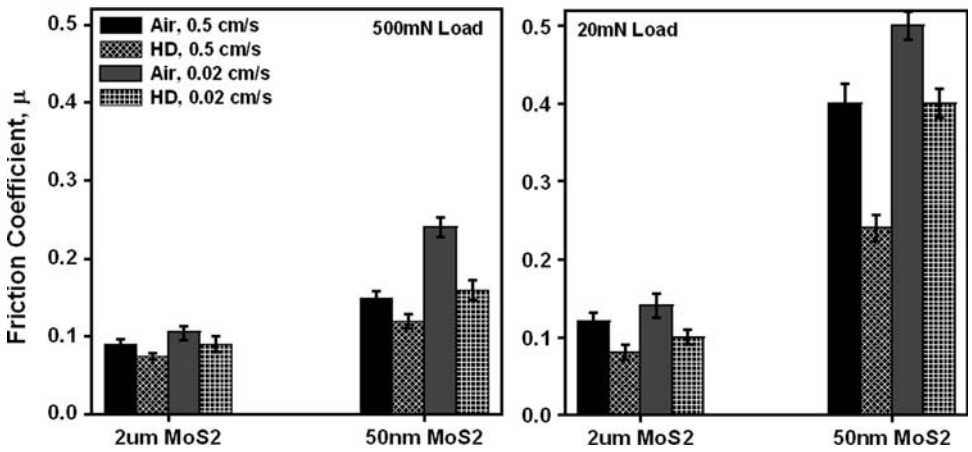

Fig. 1 Comparison in friction from MTR studies of the MoS_2 particles in air (coating) and in liquid medium (suspended in HD) for sliding speed 0.02, 0.5 cm/s and normal load 20, 500 mN. The MTR studies are done in a ball-on-flat configuration using 2-mm diameter steel ball and polished steel flats

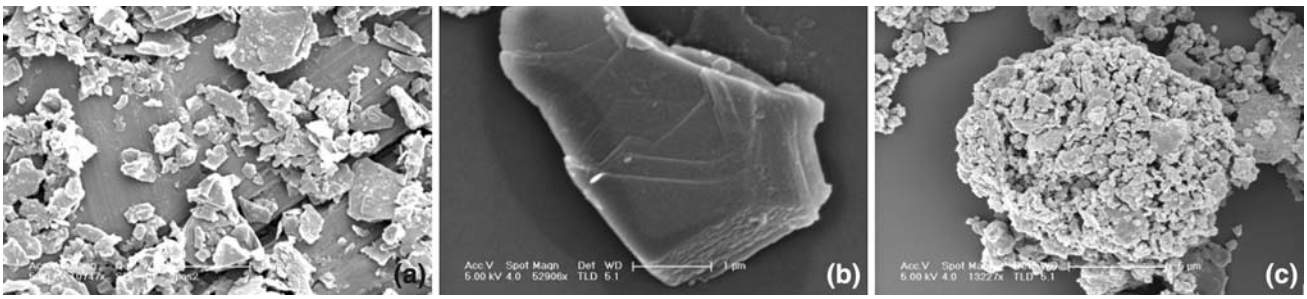

Fig. 2 SEM micrograph of **a** 2 μm, **b** large lamellar, **c** 50-nm MoS_2 particle

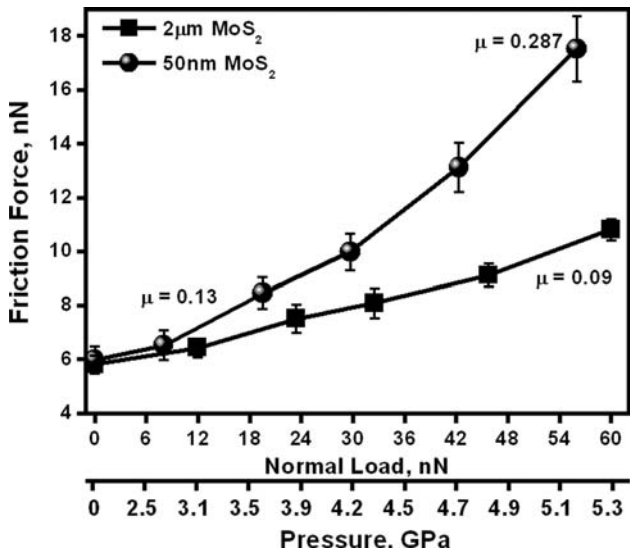

Fig. 3 LFM friction-load characteristics of bigger and smaller MoS_2 particle in ambient condition

experiment showed that even when the contact is limited to within a small area (100 × 100 nm^2 on a 2 × 2 μm^2 particle surface) at more than 100 nN normal load the whole top surface of the particle slips as a slab against the lower part of the particle. A detailed account and analysis of single particle scratching of a large MoS_2 particle is presented elsewhere [41].

Figure 4 shows the friction coefficients observed in microtribometer experiments in the ambient. In these experiments, it is observed that the friction coefficient corresponding to the large (2 μm) MoS_2 particles is consistently lower than that corresponding to the 50 nm particles, over a wide range of speed and load. The coefficient of friction at the highest speed roughly corresponds to that obtained in the AFM experiments, this suggests that when MoS_2 exists as a transfer film on the substrate the traction in a microtribometer experiment also induces basal slip.

3.1.2 *Examination of the Slid Track*

3.1.2.1 2 μm MoS_2 Particles Figure 5 shows that the large particles (as sprayed) are uniformly distributed, while the small particles stay in an agglomerated configuration, with agglomerates separated from each other, on the substrates.

Figure 6a shows that after one cycle of sliding, particles are moved by the ball such that there are, groups of particles at the two ends of the track, particles at about one-third of the width distance from the right edge and particles at the left

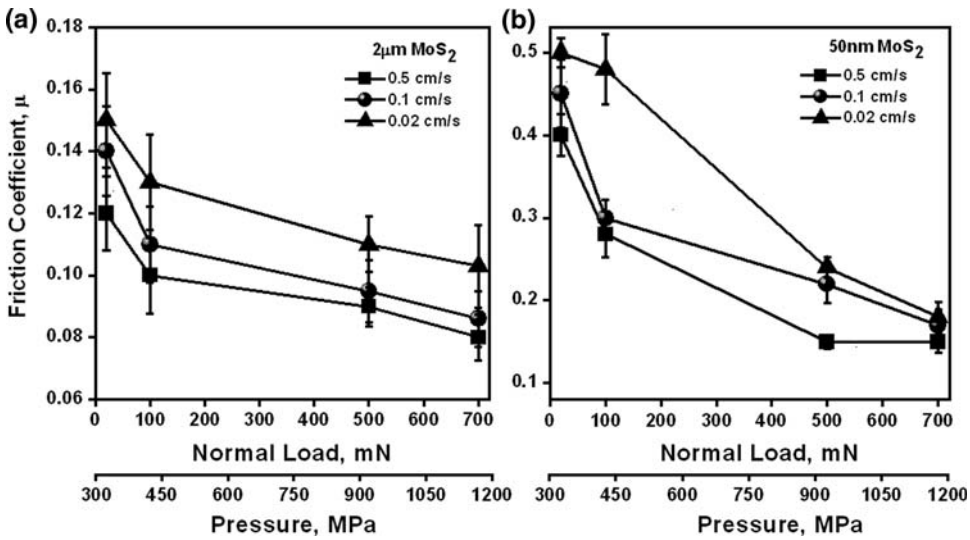

Fig. 4 Friction versus pressure (normal load) data from MTR studies of the (**a**) 2 μm and (**b**) 50 nm MoS_2 particles spin coated on steel substrate for sliding speed of 0.02, 0.1, and 0.5 cm/s

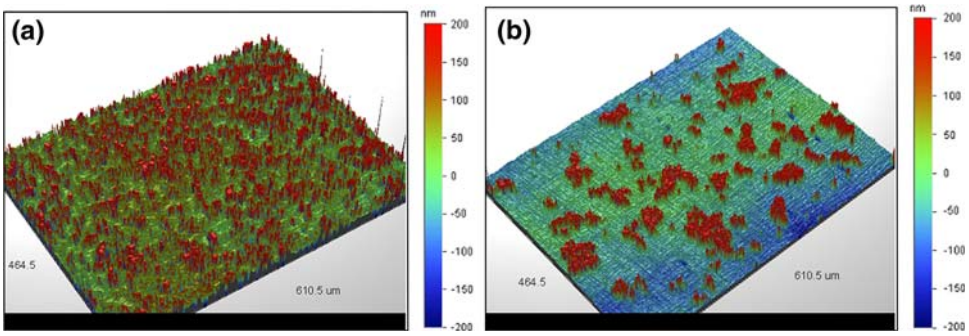

Fig. 5 3D profilometry images account the particle distribution on the steel substrate for the (**a**) 2 μm and (**b**) 50 nm MoS_2 particles

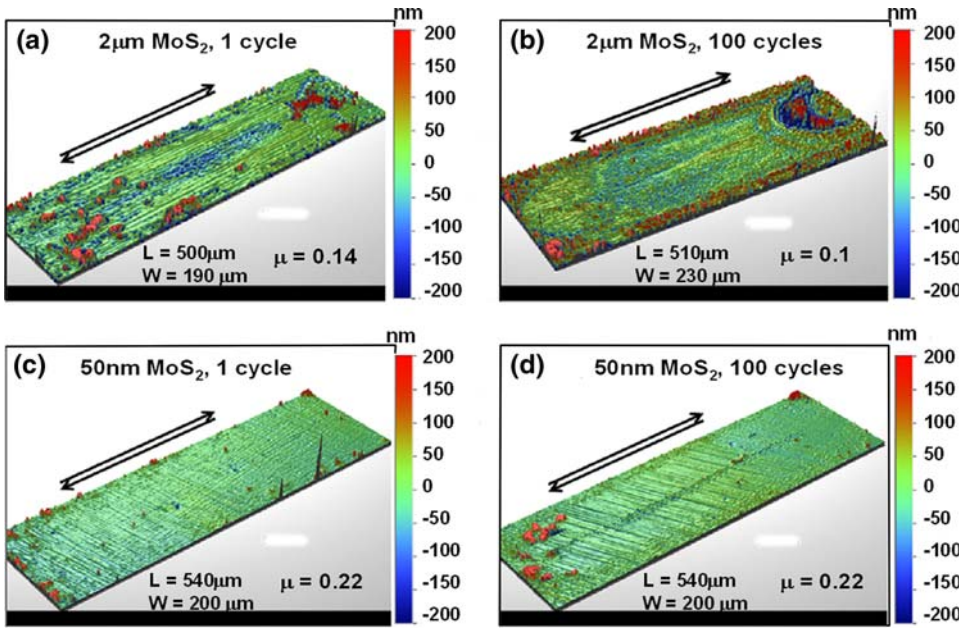

Fig. 6 3D images of the NTR tracks (100 mN, 0.5 cm/s) on steel substrate for both the particles after 1 and 100 cycles. *Arrows* indicate the sliding directions. The respective track length (*L*) and width (*W*) is specified in the figure

edge. The particles displaced toward the left edge are undeformed particles of about 400–600 nm height (Fig. 7a). Particles at the two ends are also the original particles while the ones at one-third width distance from the edge are particles, which have been sheared, to a height of about 50 nm, and compacted together to start to form a film over a 100-μm band. The rest of the substrate is abraded by the ball.

The situation changes dramatically after 100 cycles (Fig. 6b) of sliding. Loose particles are still scattered at the two extreme turn-around edges (Fig. 7b). The abrasion marks (Fig. 6a) disappear completely. With reference to Fig. 7b, we note that the strip of particles, which form at one-third distance from the edge as seen in Figs. 6a and 7a, now consolidate into a film of 100-nm height and 150-μm width in the mid-cross-sectional region of the substrate. On both sides of this region, particles appear to simply fill the abrasion marks, which are no longer seen optically but the roughness of abrasion is reproduced. The film we observe in Figs. 6b and 7b forms by further shear and compaction of the 50 nm debris (Fig. 6a) generated by shearing of the original particles and drawing in the particles from the reservoirs (Fig. 7b) situated in zones near the four edges and shearing them. As the coverage of the substrate by the film increases the coefficient of friction decreases from 0.14 after cycle 1 to 0.1 at cycle 100. Such a mechanism of film formation has been suggested earlier [26, 27].

The physical stability of MoS_2 particles, original and sheared, appears to be much influenced by the velocity of sliding. When the sliding velocity is high, the MoS_2 particles do not appear to have enough time to escape out of the contact, as succession of asperities make contact at short intervals. This helps to generate a low-friction transfer film on the substrate by the mechanism suggested above. When the speed is low, the particles can get pushed out of this contact before the next asperity has time to make contact. This leads to denudation of the substrate of MoS_2 particles. Figure 8a, b shows a film profile across and along the track when the speed is 0.5 cm/s. The corresponding profiles (Fig. 9a, b) generated at 0.02 cm/s shows a large wear crater. Sprayed MoS_2 particles thus have the ability to not only give rise to low-friction sliding, they also protect the substrate from metallic wear.

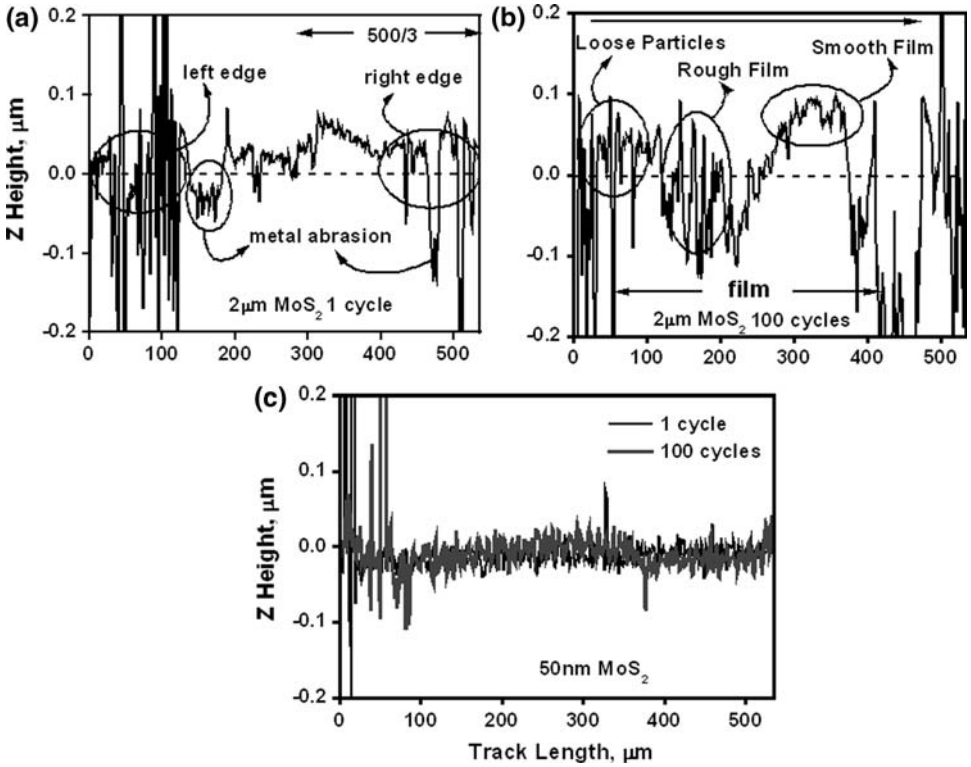

Fig. 7 The *Z* height profiles of the generated tribofilm as a function of time for the **a** 2 μm, 1 cycle, **b** 2 μm, 100 cycles, and **c** 50 nm MoS_2 particles

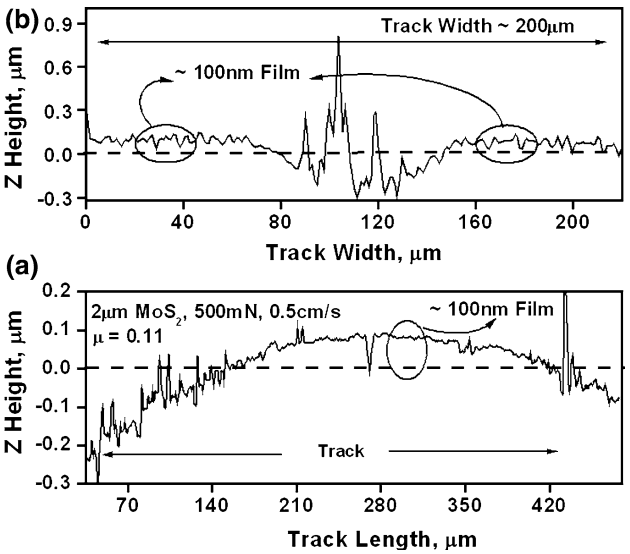

Fig. 8 The *Z* height profiles of the generated tribofilm in *X* (along the track) and *Y* (across the track) direction for 2 μm MoS_2 particles at high-speed condition (500 mN, 0.5 cm/s)

3.1.2.2 50 nm MoS_2 Particles When the substrate is sprayed with 50 nm particles, Fig. 6c shows a few agglomerates at the end of the track. The registered friction coefficient at the end of one cycle is 0.24. Few polishing marks and particles are seen on the substrate, which appears to be covered by a very thin film (optically transparent). The friction coefficient of 0.24 is well below that of a pure metal-to-metal contact. The friction coefficient does not change after 100 cycles, the corresponding substrate shows clear polishing marks, a few agglomerates at one end of the track, a fine distribution of particle/film at the other end, and a thin (~15 μm) strip of particles at the center of the track where the contact pressure is the highest. We believe that a film transferred to the counterface ball rubs partially on the grooves made by polishing and partially on the thin film of MoS_2. This gives rise to moderate friction, which is lower than metal-to-metal friction (~0.4) but higher than that obtained (0.1) when the substrate is fully covered by a MoS_2 film, as in the case when the substrate is sprayed with 2 μm MoS_2 particles.

We believe that at first contact the loose agglomerates break up into 50 nm diameter particles. On sliding even at the highest test speed a large number of particles are swept away out of the substrate leaving a substrate largely devoid of particles. Such extensive displacement takes place because the particles do not adhere well to the substrate and are perhaps easily oxidized. The high speed contact is seen in Fig. 6d to trap some third body material at the center of contact in a ~15 μm width strip. Such a strip is not seen when the speed is low. This narrow third body may indeed provide some frictional protection where the normal load and sliding speed are high. It is important to note that the coverage of the substrate by the 50 nm particles improves substantially when the normal load is increased at constant speed; compare Fig. 6d with Fig. 10b. This reduces the friction from 0.28 to 0.16 (Fig. 4). Reducing the sliding speed from 0.5 to 0.02 cm/s at 500 mN normal load

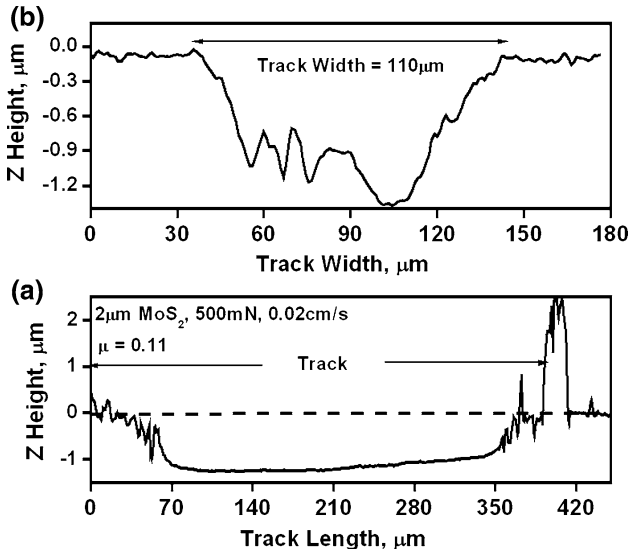

Fig. 9 The *Z* height profiles of the generated tribofilm in *X* (along the track) and *Y* (across the track) direction for 2 μm MoS_2 particles at low-speed condition (500 mN, 0.02 cm/s)

increases friction coefficient from 0.16 to 0.24, this clearly happens as the small 50 nm particles are swept away extensively from the contact at the low speed as observed by comparing Fig. 10b and c.

3.1.3 Wear Resistance

Basal slip of MoS_2 particle promotes low friction and the fact that such slip occurs in the transfer film (Figs. 3 and 4) [7, 42] explains the low frictional response of a MoS_2 film or when the particles are in liquid suspension. A more difficult question to answer is why does MoS_2 provide wear protection to the substrate when sprayed on a solid substrate. First, when the ball slides on the film, the film material, i.e., MoS_2 is removed by basal slip—this generates the debris, some of which are retained on the track and some of course leave the track. The debris on the track (see Figs. 6a and 10a) forms a reservoir, which on sliding replenishes the worn film disallowing any metal-to-metal contact. We, however, believe that the anti-wear action of MoS_2 is a little more involved. Figure 10a shows that compared to an initial Hertzian contact diameter of 40 μm, the track with MoS_2 film has a width of about 200 μm. This happens because the film is in a plastic state. Figure 11a shows pile up in a deformed film confirming its plasticity. The plastic film in this case indicates a reduction in contact pressure by about six to seven times. The wear of the film is substantially reduced due to the fall in contact pressure and the scope for deformation and consequent wear of the substrate is also reduced correspondingly. In contrast to the

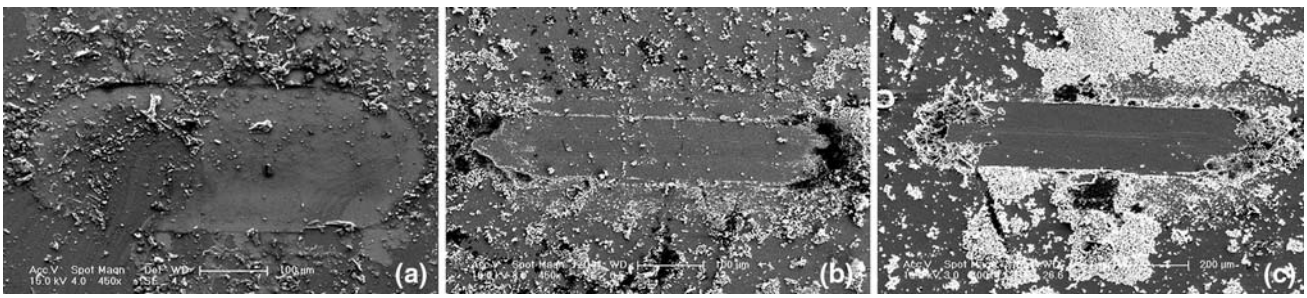

Fig. 10 SEM micrograph of the NTR tracks of **a** 2 μm MoS_2, **b** 50 nm MoS_2 particles with 500 mN load and 0.5 cm/s sliding speed, **c** 50 nm MoS_2 particles with 500 mN load and 0.02 cm/s sliding speed

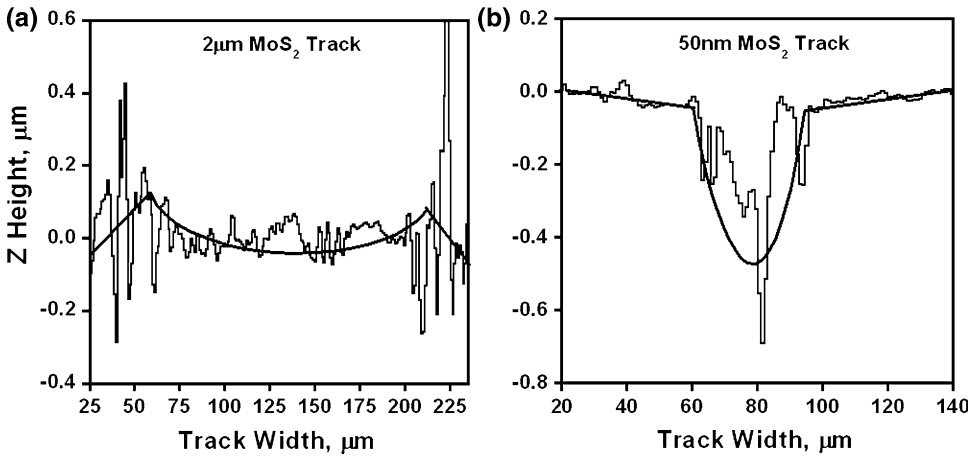

Fig. 11 Cross-sectional profile of the track (100 mN, 0.5 cm/s) formed with the **a** 2 μm and **b** 50 nm MoS_2 particles

response of the 2-μm MoS_2 film, the track formed by an inadequate film, when 50 nm particles are sprayed, has a width of about 100 μm and a groove in the track of about 40 μm width (Fig. 11b). The corresponding contact pressures are high enough to deform the substrate. Such deformation is a prerequisite for the wear of the substrate.

We report below a detailed Raman Spectroscopic analysis of the transfer film and the third body generated on the substrate by sliding the steel ball on sprayed MoS_2 particles.

3.2 Raman Spectroscopy:

There are four key first-order Raman active modes in MoS_2 [43, 44], designated as E_{1g} (286 cm^{-1}), E^1_{2g} (383 cm^{-1}), A_{1g} (408 cm^{-1}), and E^2_{2g} (32 cm^{-1}). The first three modes are due to vibration of atoms within a S–Mo–S layer. The fourth mode, E^2_{2g}, is associated with the vibration of a MoS_2 layer against neighboring layers and is called the rigid-layer mode. In backscattering experiments on a surface perpendicular to the *c*-axis, the E^2_g (286 cm^{-1}) mode is forbidden. The observed Raman spectra (Fig. 12) for the bulk MoS_2 is well matched with that observed previously (Table 1) except the E^2_{2g} mode at 32 cm^{-1}. The low frequency E^2_{2g} mode might not be clearly resolved by the present spectrometer with a relatively low energy laser source.

To identify the species on the track we perform Raman spectroscopy of some particles outside the track and some spots (Fig. 13) on the track. The spectrum of isolated 2-μm particles on the track (1 in Fig. 13a) and that of 50 nm particles inside the track (2 in Fig. 13b) are very similar to the bulk spectrum of MoS_2 (Fig. 12). When this is a film present on the substrate, the reflection from the substrate modulates the spectrum of the film in reducing intensity from that obtained from single particle MoS_2 (Fig. 13a). The intensity reduces with decreasing film thickness. For

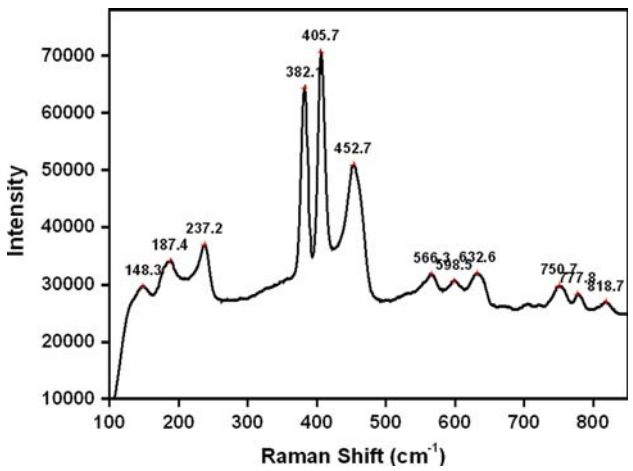

Fig. 12 Raman spectrum of bulk MoS_2 at room temperature

Table 1 Comparison between the reported Raman spectra [44] with the observed spectra for bulk MoS_2

Reported Raman shift (cm^{-1}) [44]	Raman mode	Observed Raman shift (cm^{-1})	Raman mode
32	E^2_{2g}	148.3	A
150	A	187.4	B
188	B	237.2	LA (M) [43]
286	E_{1g}	*382.1*	E^I_{2g}
383	E^1_{2g}	*405.7*	A_{Ig}
408.3	A_{1g}	452.7	C
450.2	C	566.3	$2E_{lg}$
567.3	$2E_{lg}$	598.5	D
596	D	632.6	×
750	$2E^1_{2g}$	750.7	$2E^1_{2g}$
778	E	777.8	E
816.7	$2A_{lg}$	818.7	$2A_{lg}$

The italic values are the observed main characteristic Raman shifts for the bulk MoS_2 particle at room temperature

the 2-μm particle track the film thickness was found to be 80–100 nm at position 2 and 40–50 nm at position 3. Relatively sharp peaks are, therefore, seen (Fig. 13c) for the thicker films at Raman shifts of 188, 240, 380, 408 cm^{-1}, peaks at the same shifts occur in the bulk MoS_2 samples (Table 1, Fig. 12), of course with much greater intensity. This suggests that the tribo-film on the track uphold the bulk MoS_2 configuration. Some of the peaks obtained at spots (3 in Fig 13a, c) where the film thickness is 30–40 nm occurs at the same shifts as that at spots of greater film thickness but this happens at lower intensities (Fig. 13c). The tracks corresponding to the 50-nm particle size do not in general reflect the bulk spectrum. Figure 6d shows a thin strip of material at the center of the track after 100 cycles of sliding. A Raman spectrum of this strip do not exhibit any characteristic peak of the bulk sample but a peak at 285 cm^{-1}.

The above discussion indicates that there is a MoS_2 film of varying thickness on the track made using 2 μm particles. The maximum thickness of the film ($\sim$90 nm) on the track is always significantly less than the average thickness ($\sim$300 nm) of the particles sprayed on the track. This and the spectral analysis suggest that the sheared particles constitute the track and the particles are chemically the same as the original sprayed MoS_2 particles. In contrast, no MoS_2 material either as a film or as a particle is found on the track made by rubbing the sprayed 50 nm agglomerate.

3.3 Adhesion Studies

The major difference in tribology between sprayed large (2 μm) and small (50 nm) particles may be attributed to the difference in their physical characteristics. As discussed in the introduction for a film to form, the original and sheared

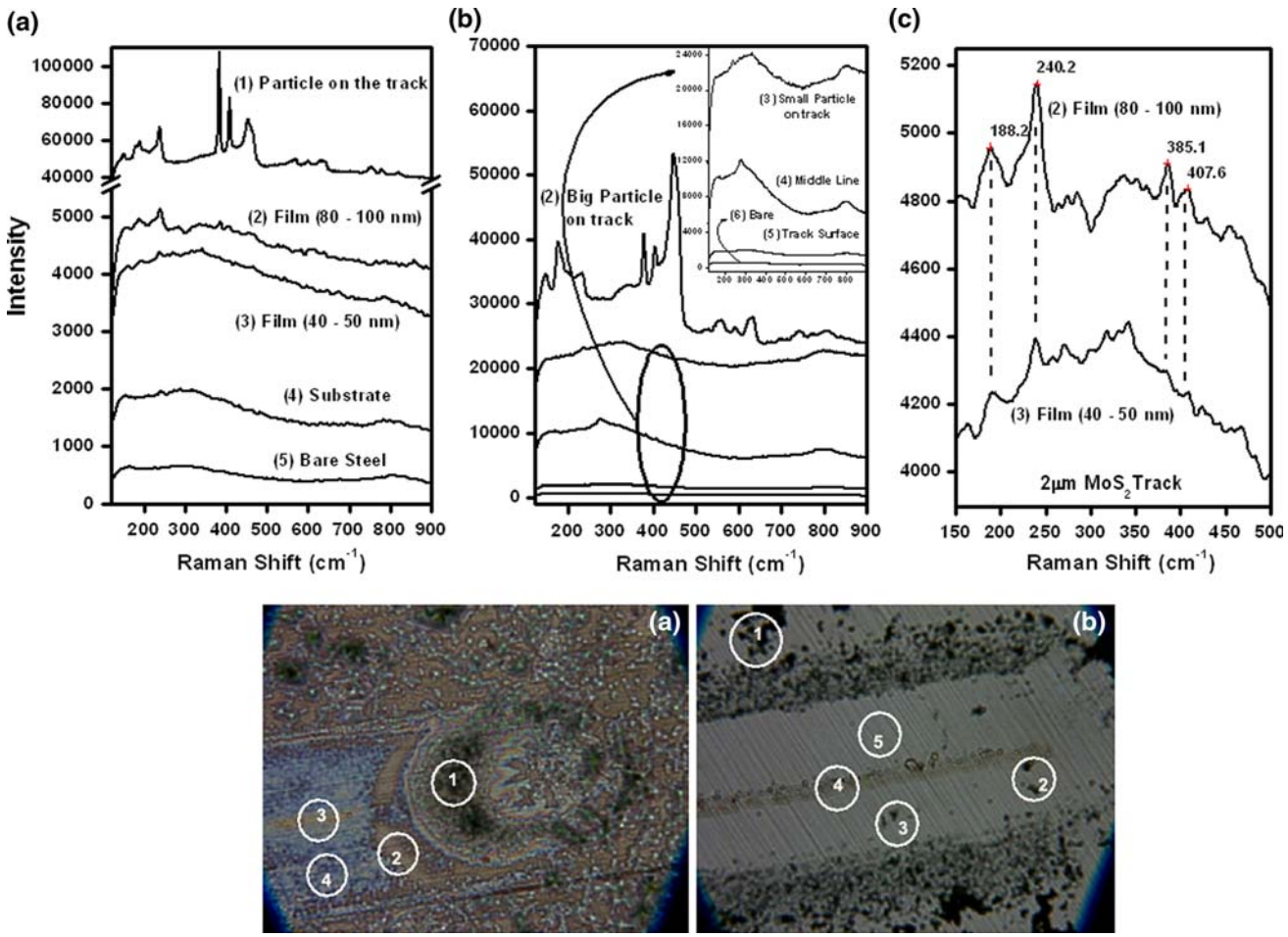

Fig. 13 Raman spectra of the shaved particle and generated tribofilm on the NTR track formed by **a** 2 μm, **b** 50 nm MoS_2 particles. The respective tracks images are shown below with the analyzed spots marked in *circles*

particles have to stick to the substrate and the counterface ball. If they do not, they are easily swept away out of contact, on sliding and no slip is possible unless at least one face of a particle is anchored. Tribological contact generates heat. In the ambient experiment, this promotes oxidation. If the particles on the substrate get heavily oxidized [2] their tribological performance is impaired, as basal slip, which is the fundamental antifriction mechanism, is inhibited. Adhesion of the particles to the substrate also deteriorates if the unsaturated bonds at the edge of the particle collect oxygen from the environment. Noting as above the superior tribology of the large MoS_2 particles, we study the adhesion and their thermal stability of the large and the small particles.

Adhesion is investigated by recording AFM force curves. The pull-off force extracted from the force curve of an AFM experiment where a Si_3N_4 tip is brought to and retracted from a single particle after contact is shown in Fig. 14. The adhesion of 2-μm particle to the SI_3N_4 tip is seen to be greater than that for the 50-nm particles. The small particles when sprayed on the surface agglomerates (Fig. 5b). We thus determined the pull off force of two particles: (1) a 20-μm size particle and (2) a 20-μm agglomerate of 50 nm particles. Figure 15a, b shows AFM image of both the particles. Figure 15c shows that the pull off force between the Si_3N_4 tip and the single particle is considerably higher than that of the tip with the agglomerate (Fig. 15d). These results are only indicative as the AFM contact is between SiO_2 and MoS_2 and not that between iron oxide and MoS_2 as it would in the micro-tribometer experiments reported above. The results indicate that the smaller particle when sprayed on the substrate stay there loosely and are unlikely to adhere strongly to a sliding track. Figures 6d and 10c infact show a large collection of 50 nm agglomerates being pushed out of contact to the edge of the track by the sliding ball.

3.4 Thermal Stability of MoS_2 Particles

In air, MoS_2 oxidizes to MoO_3 or more complex metal oxides. TGA analysis of the particles (Fig. 16) shows the oxidation potential of the 50-nm particle to be significantly higher than that of the 2-μm particles. The smaller particles

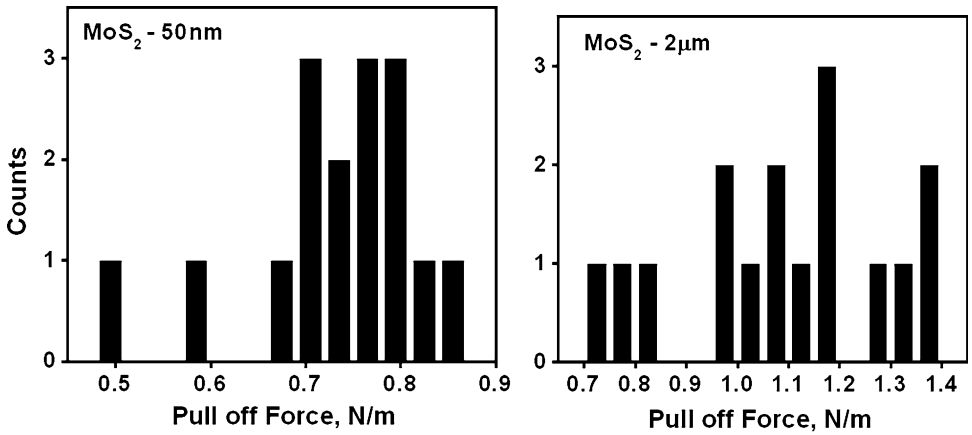

Fig. 14 AFM normalized pull-off force histogram of the smaller and bigger MoS_2 particles. Adhesion values are normalized by dividing the adhesion forces with the tip end radius

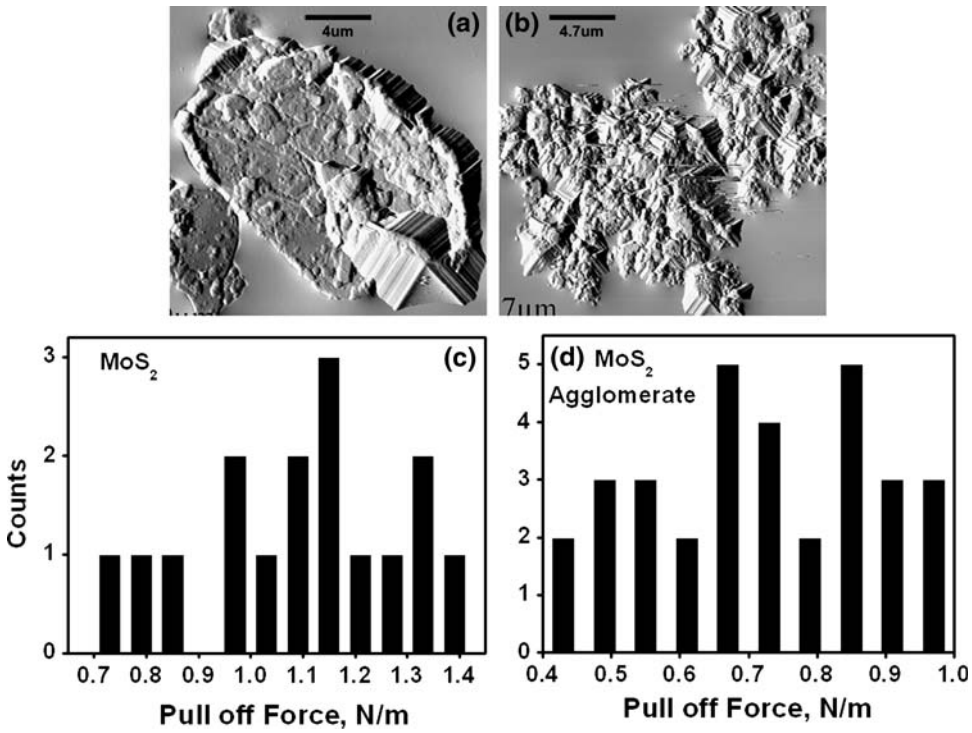

Fig. 15 AFM normalized pull off histogram of the **c** layered and **d** aggregated MoS_2 particles. The respective particle AFM images are shown above (**a**, **b**)

in contact may thus be expected to become oxidized early and loose their property to adhere to the steel surface, a condition necessary for their lubricity. The thermal stability of the MoS_2 under ambient conditions was examined by TGA, and its weight loss curve is shown in Fig. 16. The weight decrease of 2 μm particles starts at around 400 °C and is completed by 600 °C. The change represents its thermal decomposition and the ~20% weight loss in this temperature range is consistent with a conversion of MoS_2 to MoO_3 and gaseous SO_2 as reported previously [2, 45, 46]. This oxidation of MoS_2 by heating in air is believed to be dependent not only on temperature, but also on the particle size and availability of air [40]. For the 50 nm MoS_2 particle used in this study, the thermal decomposition starts at temperature 250 °C and we observe ~30% weight loss in the 250–500 °C temperature range. The oxidation temperatures for the two particle sizes used in our study are in line with the reported values of similar sized WS_2 particles [29].

4 Discussion

In this article, we have attempted to elucidate some of the basic requirements for lubrication by layered particles. We have done this by examining the contrasting performance of two particles of the same chemistry and crystallography but set apart by their two orders difference in size. We carry out ball-on-disc tribology on loosely situated particles on a ground steel substrate.

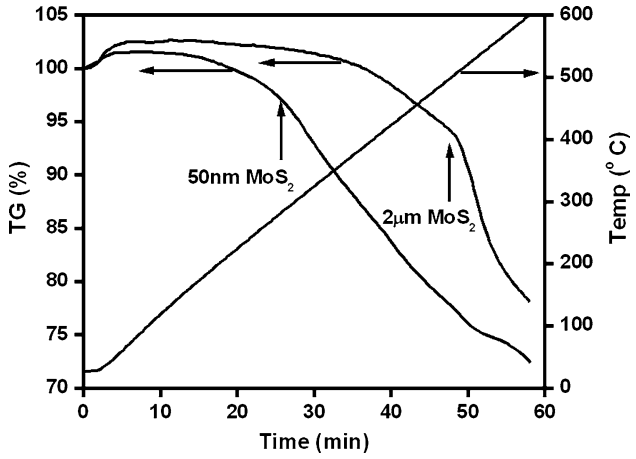

Fig. 16 Thermogravimetric (TGA) profiles of 2 μm and 50 nm MoS_2

When the particles are uniformly distributed on the substrate (Fig. 5), the first pass (Fig. 6a) removes some of the particles and pushes them into reservoirs at the turn-around or side edges of the track. In the denuded part of the track, it abrades the substrate. In the central region of the track where the contact pressure is the highest, the particles stay adhered to the substrate and are sheared. The debris generated move either to the reservoir or stay in the central part. This process presupposes that under high pressure the particles are able to adhere to the substrate and are not being swept out as it happens in the lower pressure regions and also when the particle size is small. The adhesion experiments we report (Figs. 14, 15) indicate that the big monolithic particles have an ability to adhere to oxides, whereas the agglomerate or the small particles, which may emerge from the fractured agglomerate, do not. This ability of the particle to stay in contact is crucial to tribology, we believe that the adhesion to the substrate for MoS_2 is a necessary condition but not a sufficient one. After an asperity makes contact with a single particle and shears it, the interaction may deflect the sheared particles away from the path of the next asperity if the latter does not make the contact soon enough. Thus, if the sliding speed is low, particles do not stay on the surface and the substrate is denuded of particles to promote metal-to-metal contact and wear (Figs. 8, 9). The friction coefficient is also therefore observed to be high when the sliding speed is low. Increasing the normal load appears to enhance the ability of the particle to stay on the substrate (Fig. 1) and reduce friction. There may be more than one reason for this effect and we intend to pursue this further in future using in situ Raman spectroscopy assisted tribology. In a previous article [41], we have reported that increasing the normal load shears slabs of increasing thickness, when a 20-μm particle is subjected to a shear traction, slip shear stress, however, remains insensitive to normal load. Thus, at high loads, high volumes of MoS_2 slabs are available to undertake generation and regeneration of transfer films over long sliding distances such that the incidences of metal-to-metal contact is reduced. Further, at high loads, the big slabs subjected to large contact pressures may flow and slip further at the substrate to enhance film coverage. Both these effects may contribute to the lowering of coefficient of friction by increasing the normal load as observed in Figs. 1, 4 as well as the lowering of wear as observed in Fig. 8. Without a consistent basal plane slip such mechanisms may not be available to 50 nm agglomerates. When the poorly dispersed agglomerates are on the substrate, their low adhesion to the substrate and the small size appear to encourage deflection of the particle away from contact even at high sliding speeds.

Beyond the first pass, the sliding process builds on the initial strip of 50-nm sheared particles in the central region of the substrate. Particles from the reservoir (Figs. 6b, 10a) are drawn into the contact dynamically to increase the height, width, and length of this central region (Figs. 7b, 8). By the time 100 cycles of sliding are over, the maximum height increases to about 100 nm and the particles are uniformly (as seen optically) smeared over the whole track. The Raman spectroscopy of this track (Fig. 13) establishes that the track now consists of materials, which are chemically the same as the original MoS_2 particle. In conjunction with profilometry, the spectroscopy however establishes that the film, which forms on the track is non-uniform in thickness, thickest in the central region and thinnest (Fig. 13) at the edge of the track. It is also seen (Fig. 8) that at the turn-around regions where the sliding velocity is low, the film is thin. Thus, a crown-shaped film forms on sliding of 2 μm MoS_2 particles.

How does the film form? We have not examined the counterface ball in any detail but have observed transfer films on it throughout the experimental duration. We believe that the particle in the substrate track and the counterface are perpetually sheared exposing the basal plane. The fact that the friction coefficient observed in the microtribometer experiment (Fig. 4) is of the same order as that observed when a basal slip was engineered in a LFM experiment on a single MoS_2 particle (Fig. 3), suggests that all activities on the track are due to basal slip of the MoS_2 particles. Wahl et al. [27] on the basis of their in situ Raman tribometry of deposited MoS_2 come to the same conclusion. The slip transfers part of a particle to the counterface, which when further sheared comes to the track and pressed along with the particles already on the track and drawn from the reservoir of loose particles, form the film. The shape of the film on the track appears to be strongly influenced by the profile of pressure distribution on the counter face ball and the velocity profile along the track.

One of the most important finding of this present study is the ability of this original loosely sprayed particles to

promote wear resistance to the substrate. Once the film forms, though nonuniform in thickness and shape over the track, it appears to be remarkably homogenous. Under traction, the film deforms in a state of plasticity (Fig. 11). The plasticity expands the contact area (Fig. 10) to the point that the contact pressure is reduced significantly to discourage subsurface deformation of the substrate and the resulting wear. While most of the track is covered by the protective film, incidence of metal-to-metal contact especially in the very high-pressure region cannot be ruled out (viz, see the very rough region at the middle of the track in Fig. 8a). The heat generated by traction can oxidize the particle, this may be deleterious to the formation of a uniform film. Our thermal stability study shows that the large MoS_2 particles are thermally stable (Fig. 16) and are not prone to oxidation at modest temperatures. We thus expect a stable and protective nonuniform MoS_2 film to form on the steel surface when uniformly distributed loose particles on steel surface are rubbed by a steel ball.

The ability of a particle to migrate to and to stay at the contact appears to be the principal requirements for good tribological performance of the layered dichalcogenides. Within present tractional conditions, it is this consideration, which distinguishes the tribology of large and small MoS_2 particles. While this may be true, we believe that the behavior of very small particles in tribology is not fully understood. These particles if allowed to migrate and stay at contact are likely to give rise to very thin (transparent) sheared slivers. These slivers may be chemically active to react with the substrate and the counterface to yield compounds, which may be tribologically useful. We have some indication of this from the present work where we note friction coefficients for 50 nm particles, which are significantly lower than that of metal-to-metal contact despite the fact that most of the particles appear to have been swept away by sliding. The Raman spectroscopy results indeed suggest that these slivers may contain a new reaction product on the track, created by sliding of sprayed 50 nm particles. This compound and its properties need to be explored in the future. Present work thus indicates the possibility of obtaining good tribological property with nanoparticles where such particles may be made useful by enhancing the sliding speed and the contact pressures.

5 Conclusion

Molybdenum disulfide nanoparticles are sprayed on a smooth steel substrate and slid against a steel ball. The ability of the particles to form a low-friction transfer film on the substrate is found to be crucially related to their ability to stay at the contact. This ability is further related to their size, their adhesion to the substrate, oxidation potential as well as on operating parameters such as normal load and sliding velocity. These factors influence the formation of a nonuniform homogeneous film when the particles are large (2 μm), the film under traction is plastic. Large contact areas are generated to modulate contact pressures to provide wear protection. The small 50 nm particles are unable to migrate to the contact under traction to undergo basal slip, the mechanism necessary for the formation of debris and the film. The friction of the small particles is therefore found to be, within the present range of load and speed, significantly higher than that observed for the large particles.

In this work, we also observe a strong effect of normal load on coefficient of friction, especially when large 2-μm monolithic MoS_2 are sprayed on the steel substrate and slid against a steel ball. We suggest that this happens because the thickness of the slabs sheared at contact increases with normal load. This aids the formation of a stable transfer film as well as it enhances the coverage of the substrate by the MoS_2.

Acknowledgment The authors are grateful to Hindustan Petroleum Corporation Limited (HPCL), Mumbai, India for their support in carrying out this work. Our sincere thanks to Mrs. Bindu CN, for the help in carrying out this work.

References

1. Bowden, F.P., Tabor, D.: The Friction and Lubrication of Solids, Part II. Oxford University Press, London (1964)
2. Bhushan, B., Gupta, B.K.: Handbook of Tribology. McGraw-Hill, New York (1991)
3. Black, A.L., Dunster, R.W., Sanders, J.V.: Comparative study of surface deposits and behavior of MoS_2 particles and molybdenum dialkyl-dithio-phosphate. Wear **13**, 119–132 (1969)
4. Gansheimerand, J., Holinsky, R.: A study of solid lubricants in oils and greases under boundary conditions. Wear **19**, 439–449 (1972)
5. Bell, M.E., Findlay, J.H.: Molydenite as a new lubricant. Phys. Rev. **59**, 922–927 (1941)
6. Braithwaite, E.R., Rowe, G.W.: Principles and applications of lubrication with solids. Sci. Lubr. **15**, 92–96 (1957)
7. Winer, W.O.: Molybdenum disulphide as a lubricant: a review of the fundamental knowledge. Wear **10**, 422–452 (1967)
8. Spalvins, T.: Morphological and frictional behavior of sputtered MoS_2 films. Thin Solid Films **96**, 17–24 (1982)
9. Holinski, R., Gansheimer, J.: A study of the lubricating mechanism of molybdenum disulphide. Wear **19**, 329–342 (1972)
10. Buck, V.: Morphological properties of sputtered MoS_2 films. Wear **91**, 281–288 (1983)
11. Fleischauer, P.D., Tolentino, L.U.: Effects of crystallite orientation on the environmental stability and lubrication properties of sputtered MoS_2 thin films. ASLE Trans. **27**, 82–88 (1984)
12. Roberts, E.W.: Thin solid lubricants in space. Tribol. Int. **23**, 95–105 (1990)
13. Miyoshi, K., Honecy, F.S., Abel, P.B., Pepper, S.V., Spalvins, T., Wheeler, D.R.: A vacuum (10–9 Torr) friction apparatus for determining friction and endurance like that of MoS_x films. Tribol. Trans. **36**, 351–358 (1993)

14. Suzuki, M.: Comparison of tribological characteristics of sputtered MoS_2 films coated with different apparatus. Wear **218**, 110–118 (1998)
15. Wang, D.Y., Chang, C.L., Chen, Z.Y., Ho, W.Y.: Microstructural characterization of MoS_2-Ti composite solid lubricating films. Surf. Coat. Technol. **121**, 629–635 (1997)
16. Killeffer, D.H., Linz, D.: Molybdenum Compounds: Their Chemistry and Technology. Interscience, New York (1952)
17. Bowden, F.P., Tabor, D.: Friction: An Introduction to Tribology, vol. 91. Anchor, Garden City, NY (1973)
18. Singer, I.L.: Solid lubrication processes. In: Singer, I.L., Pollock, H.M. (eds.) Fundamentals of Friction: Macroscopic and Microscopic Processes. Kluwer, Dordrecht (1992)
19. Dickinson, R.G., Pauling, L.: The crystal structure of molybdenite. J. Am. Chem. Soc. **45**, 1466–1471 (1923)
20. Bragg, W.: The investigation of the properties of thin films by means of x-rays. Nature **115**, 266–269 (1925)
21. Waghray, H., Lee, T.-S., Tatarchuk, B.J.: A study of the tribological and electrical properties of sputtered and burnished transition metal dichalcogenide films. Surf. Coat. Technol. **77**, 415–420 (1995)
22. Schumacher, A., Kruse, N., Prins, R., Meyer, E., Lüthi, R., Howald, L., Güntherodt, H.-J., Scandella, L.: Influence of humidity on friction measurements of supported MoS_2 single layers. J. Vac. Sci. Technol. B **14**, 1264–1267 (1996)
23. Prasad, S.V., Zabinski, J.S.: Tribology of tungsten disulphide (WS_2): characterization of wear-induced transfer films. J. Mater. Sci. Lett. **12**, 1413–1415 (1993)
24. Singer, I.L.: Mechanics and chemistry of solids in sliding contact. Langmuir **12**, 4486–4491 (1996)
25. Fayeulle, S., Ehni, P.D., Singer, I.L.: Analysis of transfer films formed on steel and co-WC during sliding against MoS_2-coated steel in argon. Surf. Coat. Technol **41**, 93–101 (1990)
26. Wahl, K.J., Singer, I.L.: Quantification of a lubricant transfer process that enhances the sliding life of a MoS_2 coating. Tribol. Lett. **1**, 59–66 (1995)
27. Wahl, K.J., Belin, M., Singer, I.L.: A triboscopic investigation of the wear and friction of MoS_2 in a reciprocating sliding contact. Wear **214**, 212–220 (1998)
28. Rapoport, L., Bilik, Yu., Feldman, Y., Homyonfer, M., Cohen, S.R., Tenne, R.: Hollow nanoparticles of WS2 as potential solid-state lubricants. Nature **387**, 791–793 (1997)
29. Rapoport, L., Feldman, Y., Homyonfer, M., Cohen, S.R., Solan, J., Hutchison, J.L., Tenne, R.: Inorganic fullerene-like material as additives to lubricants: structure–function relationship. Wear **225–229**, 975–982 (1999)
30. Tenne, R., Margulis, L., Genut, M., Hodes, G.: Polyhedral and cylindrical structures of tungsten disulphide. Nature **360**, 444–446 (1992)
31. Feldman, Y., Wasserman, E., Srolovitz, D.J., Tenne, R.: High-rate gas-phase growth of MoS_2 nested inorganic fullerenes and nanotubes. Science **267**, 222–225 (1995)
32. Rapoport, L., Leshchinsky, V., Lvovsky, M., Nepomnyashchy, O., Volovik, Y., Tenne, R.: Mechanism of friction of fullerenes. Ind. Lubr. Tribol. **54**, 171–176 (2002)
33. Joly-Pottuz, L., Martin, J.M., Dassenoy, F., Belin, M., Montagnac, G., Reynard, B., Fleischer, N.: Pressure-induced exfoliation of inorganic fullerene-like WS_2 particles in a Hertzian contact. J. Appl. Phys. **99**, 023524 (2006)
34. Devaprakasam, D., Khatri, O.P., Shankar, N., Biswas, S.K.: Boundary lubrication additives for aluminium: a journey from nano to macrotribology. Tribol. Int. **38**, 1022–1034 (2005)
35. Green, C.P., Lioe, H., Cleveland, J.P., Proksch, P., Mulvaney, P., Sader, J.E.: Normal and torsional spring constants of atomic force microscope cantilevers. Rev. Sci. Instrum. **75**, 1988–1996 (2004)
36. Cleveland, J.P., Manne, S., Bocek, D., Hansma, P.K.: A nondestructive method for determining the spring constant of cantilevers for scanning force microscopy. Rev. Sci. Instrum. **64**, 403–404 (1993)
37. Ogletree, D.F., Carpick, R.W., Salmeron, M.: Calibration of frictional forces in atomic force microscopy. Rev. Sci. Instrum. **67**, 3298–3306 (1996)
38. Gubarevich, A.V., Usuba, S., Kakudate, Y., Tanaka, A., Odawara, O.: Frictional properties of diamond and fullerene nanoparticles sprayed by a high-velocity argon gas on stainless steel substrate. Diam. Relat. Mater. **14**, 1549–1555 (2005)
39. Moshkovith, A., Perfiliev, V., Cyclesker, I., Fleischer, N., Tenne, R., Rapoport, L.: Friction of fullerene-like WS_2 nanoparticles: effect of agglomeration. Tribol. Lett. **24**, 225–228 (2006)
40. Farr, J.P.G.: Molybdenum disulphide in lubrication: a review. Wear **35**, 1–22 (1975)
41. Sahoo, R.R., Math, S., Biswas, S.K.: Mechanics of deformation under traction and friction of a micrometric monolithic MoS_2 particle in comparison with those of an agglomerate of nanometric MoS_2 particle. Tribol. Lett. (2009). doi:10.1007/s11249-009-9504-9
42. Martin, J.M., Donnet, C., Le Mogne, Th., Epicier, Th.: Superlubricity of molybdenum disulphide. Phys. Rev. B **48**, 10583–10588 (1993)
43. Wieting, T.J., Verble, J.L.: Infrared and Raman studies of long-wavelength optical phonons in hexagonal MoS_2. Phys. Rev. B **3**, 4286–4292 (1971)
44. Chen, J.M., Wang, C.S.: Second order Raman spectrum of MoS_2. Solid State Comm. **14**, 857–860 (1974)
45. Wong, K.C., Lub, X., Cotter, J., Eadie, D.T., Wong, P.C., Mitchell, K.A.R.: Surface and friction characterization of MoS_2 and WS_2 third body thin films under simulated wheel/rail rolling–sliding contact. Wear **264**, 526–534 (2008)
46. Allam, I.M.: Solid lubricants for applications at elevated temperatures. J. Mater. Sci. **26**, 3977–3984 (1991)